American Mineralogist, Volume 84, pages 629–638, 1999

Surface chemical characterization and surface diffraction effects of real margarite (001): An angle-resolved XPS investigation

GIUSEPPE G. BIINO,[1,2]* NORMAN MANNELLA,[2,3] ALEXANDER KAY,[2,3] BONGJIN MUN,[2,3] AND CHARLES S. FADLEY[2,3]

[1]Asylum for too Advanced Earth Scientists, Le Pavillon, Zimmerwald 3086, Switzerland
[2]Materials Sciences Division, Lawrence Berkeley National Laboratory, Berkeley, California 94720, U.S.A.
[3]Physics Department, University of California-Davis, Davis, California 95616, U.S.A.

ABSTRACT

The (001) surface of natural pure margarite was chemically characterized by angle-resolved X-ray photoelectron spectroscopy (ARXPS). The extreme surface sensitivity of ARXPS permits concluding that the chemical composition of the near-surface region differs from the bulk because of the strong anisotropy of the margarite structure. Depth profiling was carried out by angle resolved spectroscopy that is a non destructive measuring technique. More grazing polar angles sample increasingly superficial layers of the margarite. The topmost layers are made up of C, due to the mineral/atmosphere interaction. At low grazing angles the concentration of Si increases, and both Al and Ca decreases; therefore we conclude that the tetrahedral sheet is the topmost monolayer. Repulsion between the octahedral and tetrahedral sheets is probably responsible for the cleavage. Photoelectron diffraction effects are also clearly evidenced by Si, Ca, and Al. Single-scattering cluster calculations were performed in simulating scanned angle core emission. The calculated patterns do not show a reasonable agreement with experimental data.

INTRODUCTION

Margarite mica [$CaAl_2(Al_2Si_2)O_{10}(OH)_2$] occurs in Al- and Ca-rich metamorphic rocks (Bucher-Nurminen et al. 1983; Bucher and Frey 1994; Feenstra 1996). Despite a large *P-T* stability field (Chatterjee 1974, 1976), margarite is rare and has received little attention (Guggenheim and Bailey 1978; Guggenheim 1984). Yet, margarite completes the crystallochemical analogy between feldspar and micas and has a well-ordered Si-Al tetrahedral sheet. Cleavage along (001) is very poor and consequently it is a brittle mica. This mechanical property, atypical for a mica, arises from the strong Ca-O chemical bond. The cleavage mechanism has never been investigated, whereas it is generally believed (Giese 1974, 1977, 1978, 1984) that cleavage of K- or Na-bearing micas results in the exposure of these interlayer cations.

We did not investigate a clean margarite surface (in surface science a clean surface means absence of foreign matter sorbed on the lattice termination), but a real margarite surface (in surface science a real surface means that some of the dangling bonds making the lattice termination are satisfied by atoms, molecules, or molecules fragments sorbed mainly during gas-solid interactions during standard laboratory preparation), because it is more close to a natural surface. One aim of this investigation is to provide experimental evidence for the cleavage mechanism by better defining the structural termination of a cleaved real margarite crystal. The reconstruction of a crystal termination is not an academic curiosity, because chemically reactions of solids evolve according to chemistry and structure of the topmost layers. Consequently, improved characterization of the surface chemistry and surface structure of margarite is relevant to research fields such as environmental sciences.

A principal method for surface chemical analyses is X-ray photoelectron spectroscopy (XPS), which measures the kinetic energy of photoelectrons emitted. It is a surface sensitive tool because such photoelectrons have short inelastic mean free paths (IMFP) in solids. The kinetic energy of the electrons gives direct information on the energy of binding, the chemical composition of the outermost layers of the sample, oxidation states, and indirectly also coordination environments. Depth distribution of atoms is probed using the angular dependence of the emission (ARXPS). Finally, atomic structure information is contained in photoelectron diffraction effects due to elastic scattering of electron by atoms neighboring the emitter (Fadley 1992; Chambers 1992; Osterwalder et al. 1995; Biino et al. 1998).

The present work uses ARXPS to investigate the following questions: (1) Does the surface chemical composition of cleaved (001) margarite correspond to the bulk chemical composition or does the ARXPS surface sensitivity make it impossible to probe a volume large enough to be representative of the bulk composition? (2) The photoelectrons emerging from the (001) of margarite should undergo diffraction that may change the intensity at different angles of the outgoing photoelectron. ARXPS measurements were thus also performed at different polar angles (i.e., the angle, θ, measured between the sample surface and the analyzer) to investigate if these dif-

*E-mail: ggbiino@access.ch

0003-004X/99/0004–0629$05.00

fraction effects are important for this system. (3) Can single-scattering cluster (SSC) calculations of core-level polar X-ray photoelectron diffraction (using as model the bulk lattice) be in reasonable agreement with experimental data?

MARGARITE CRYSTAL CHEMISTRY

Margarite was chosen for this methodological study because the mineral shows a well-defined layered structure, has negligible cation substitutions, and Al is present in a strictly fixed stoichiometry, in two different lattice positions. This provides a very simple structural model to explore via ARXPS investigation.

The structure of micas is traditionally described as layers of alternating tetrahedra-octahedra-tetrahedra, the T-O-T layer. In end-member brittle micas, two Al atoms and two Si atoms per formula unit (pfu) are in tetrahedral coordination, and therefore the T-O-T layer charge pfu is -2.0. Consequently, the charge unbalance in the tetrahedral sheet is balanced by the interlayer cation that must have charge 2^+. Divalent cations also must keep the T-O-T layer properly split, and therefore only a few divalent cations are present in brittle micas. Ca and/or Ba properly satisfy the required radius and charge conditions.

For the purpose of this work, the margarite structure is best described by a repetition of 8 monolayers: an O monolayer, a Si-Al monolayer, an O monolayer, an Al monolayer, an O monolayer, a Si-Al monolayer, an O monolayer, and a Ca monolayer as shown in Figure 1.

SAMPLE DESCRIPTION AND PREPARATION

We investigated a well-characterized pure margarite from monomineralic vinelets in marble on the island of Naxos (Feenstra 1996). A centimeter diameter margarite monocrystal was cleaved in air with a sharp cutter and shaped to fit the sample holder. The investigated (001) face was microscopically flat. Microscopic inspection of the crystals also did not show evidence of any inclusions. Margarite cleaving is not perfect, and we were only able to prepare a microscopically flat surface handling it in air. Because surface roughness may alter the angle resolved results (Fadley et al. 1974) we paid extremely close attention in the preparation of a flat surface. The cleaved crystal was fixed using an ultrahigh vacuum glue on a gold sample holder. The *b* axis of the crystal was roughly oriented parallel to the rotation axis of the manipulator. Two samples of the same crystal were investigated. One sample was measured at each 10° step in polar angle, and the second sample at each 5° step. These two samples gave identical results, and therefore in the following we will discuss only the most complete set of experiments with 5° steps.

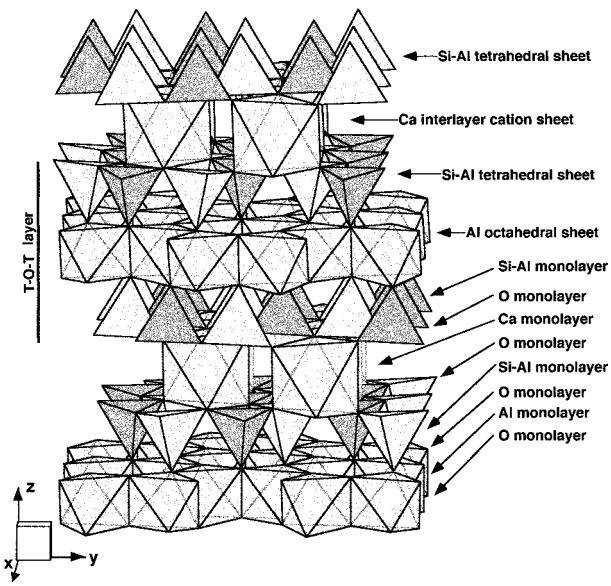

FIGURE 1. Perspective view of the ideal crystal structure of margarite. The nomenclature of the monolayers is given.

TABLE 1. Chemical states table

Orbital	E_B	FWHM
Al2p	74.32	1.89
Si2p	102.36	1.99
C1s	284.99	2.11
$Ca2p_{3/2}$	348.56	2.19
O1s	531.79	2.40

Notes: The binding energy (E_B) and full width at half maximum peak hight above background (FWHM) are given in electron volts (eV). The binding energy are after charge correction. The charge was corrected to Si_{2p} line at 102.36 eV (after Biino and Gröning 1998a).

ANALYTICAL TECHNIQUE AND MEASURING PROCEDURES

Several introductory reviews of quantitative surface analysis by XPS are available and we will subsequently make use of various results from them (Fadley 1978; Briggs and Seah 1990; Hufner 1995; Tilinin et al. 1996).

This investigation was carried out with a refurbished Hewlett-Packard 5950A X-ray photoelectron spectrometer at the Department of Physics of the University of California, Davis. All the spectrometer specifications are given in Baird (1977). The spectrometer sample holder allows angle-resolved measurements because the polar angle can be varied. The (001) surface micas was irradiated with monochromatized Al*K*α (hν = 1486.6 eV) radiation that traversed a thin beryllium window separating the X-ray tube from the main spectrometer chamber. Spectra were taken with the standard 115 eV pass energy and a 0.2 eV channel width in each spectrum. The X-ray source was operated at 800 W. During measurement the pressure was ca. 2×10^{-9} torr. The energy scale of the spectrometer was calibrated to the $4f_{7/2}$ peak of Au at a binding energy (E_B) of 84.0 eV.

We measured core photoelectron spectra of all pertinent elements except H (which cannot be seen by XPS). Interlayers made up of muscovite and paragonite are rather common in margarite (Feenstra 1996), and therefore we also always monitored K and Na. However Ba, K, and Na were never detected, a large amount of C was seen, probably because dangling bonds are created by cleavage, and they instantaneously react with atoms, molecules, and fragment of molecules present in the atmosphere. CO and CO_2 molecules were not detected. It is probable that O contamination also occurred, but due to the O1s peak complexity we cannot resolve it. Atomic concentra-

tions were calculated from intensity of the Al2p, Ca2p, Si2p, O1s, and C1s photoelectrons.

PHOTOELECTRON ELECTRON SPECTRA AND PEAK POSITION

Figure 2 illustrates the kind of photoelectron spectra obtained. Surface contamination due to an air-margarite interaction is well evident (i.e., C1s), but any natural margarite crystal exposed to air has this contamination too.

Margarite is a good insulator and its surface thus becomes positively charged during photoemission, shifting down peaks on average by ca. 10.87 eV. Several charge correction techniques are currently used, each of which has merits and pitfalls (Seah 1990). Because precise peak position is not important, we simply use the Si2p at E_B = 102.36 eV as an internal peak reference following Biino and Groening (1998a). The binding energy of all analyzed elements after charge correction are given in Table 1. The measured value of the Al2p differs from the literature Al2p value in micas of only 0.1 eV (74.25 eV, Wagner et al. 1982; Biino and Groening 1998a). The measured value of the C1s after correction indicates C is present as adsorbed hydrocarbons.

DATA TREATMENT

The difference between the measured energy distribution and the background can be used to derive chemical compositions of the surface and near-surface region of solids. The background is caused by the electrons that have undergone multiple inelastic scattering and lost energy (i.e., they do not contribute to the characteristic elastic peak intensity). Consequently, the attenuation of the elastic signal is mainly due to electron inelastic collisions, and it is necessary to know the electron sampling depth to gain the chemical composition of the sample.

The term attenuation length (AL) was originally used for this purpose. This paper provides evidence for elastic scattering, therefore AL is not the most appropriate model (see also Tanuma et al. 1993 and reference therein). Instead, IMFP were used. We first consider only the IMFP (defined as the average of distances, measured along trajectories, that electrons with a given energy travel between inelastic collision in a substance). IMFP were determined based on the empirical approach of Seah and Dench (1979), who fitted all available IMFP values of solids to a universal curve. The single universal curve is a convenient approximation and is valuable in cases where there are no measurements, but IMFP are material dependent and can only be described by a single universal curve as a function of energy as a first approximation. It is impossible to assess the accuracy of the single universal curve, and the conditions under which it might break down are not known. Using Seah and Dench's (1979) approach, λ_{SD} (in number of monolayers) is 12.98 (Al2p), 11.66 (Ca2p), 12.84 (Si2p), and 10.65 (O1s), and the average thickness d_{SD} of each monolayer in maragite is 2.29 Å.

Second, we followed a more complete theoretical approach, after Penn (1987), who proposed a hybrid approach to calculate IMFP values based on experimental and theoretical data. Information on the inelastic scattering probability as a function of energy loss for each material is gained from experimental optical data. The optical data can be checked for internal consistency (although internal consistency does not imply accuracy). The algorithm proposed by Penn (1987) neglects vertex corrections, self-consistency, and the effects of exchange and correlations. We used the predictive formula TPP-2 for the IMFP calculation by Tanuma et al. (1993), which incorporates Penn's algorithm (1987). TPP-2 was constructed by fitting the calculated IMFP values for elements and substances to a modified form of the Bethe equation for inelastic electron scattering in matter. These authors suggested that the four parameters in the Bethe equation can be related empirically to: atomic or molecular weight, bulk density, number of valence electrons per atom or molecule, and band-gap energy for non-conductors. We considered that margarite has a band gap energy of 9.0 eV (approximated from the Al_2O_3 and SiO_2 band gaps). At the photon energy of 1486.6 eV, a change of 1 eV in band gap energy causes a change in the IMFP of approximately 1 Å. Using TPP-2, we calculate that the IMFP value is 28.51 Å (Al2p), 24.09 Å (Ca2p), 27.87 Å (Si2p), and 20.85 Å (O1s). These values were used in solving Equation 6, below. It is also known that multiple scattering and damping effects make the real net distance traveled by the electrons less than the calculated IMFP. Due to the exponential dependence of photoelectron transport to the surface, 85% of the ARXPS signal originates from a surface region with 2λ thickness and 95% of the signal originates within the 3λ region from a surface region, for normal emission.

The chemical surface analysis can be calculated following the approach by Fadley et al. (1974) and Fadley (1978). To calculate the transport of the photoelectrons to the surface, we model the margarite structure as a regular sequence of monatomic layers laterally homogeneous in composition. We assume that surface relaxation and surface reconstruction did not occur after cleavage and during analysis, and model the crystal as two main layers: the true margarite (substrate) and an overlayer of contaminants. The surface is covered by a layer of contaminants due to atmosphere-margarite reaction after cleaving. The contaminant cannot be removed by sputtering because it causes perturbation of the mineral surface (Hochella et al. 1988; Biino and Gröning 1998a, 1998b). Consequently, the signal is attenuated by a factor T_c, calculated as in the following

$$T_c = \exp(-d_c/\lambda_c \sin\theta) \quad (1)$$

where d_c is the thickness of the contaminant overlayer, λ_c is the electron IMFP, and θ is the polar angle. The different IMFP values were chosen considering the IMFP of graphite (λ_c = 22 Å, Martin et al. 1985) and of glassy C (λ_c = 26 Å, Powell et al. 1994). The experimental thickness of C overlayer on minerals is probably, to a first approximation, 10 Å (Stipp and Hochella 1991; Junta Rosso and Hochella 1996). The attenuation correction is important at low polar angle where the C makes up large part of the analyzed surface. Carbon density was calculated from the following formula

$$I_c(\mathrm{C1s},\theta) = K\rho_c \frac{d\sigma_{(\mathrm{C1s})}}{d\Omega}[1-\exp(-d_c/\lambda_c \sin\theta)] \quad (2)$$

where I_c (C1s,θ) is the number of photoelectrons per second

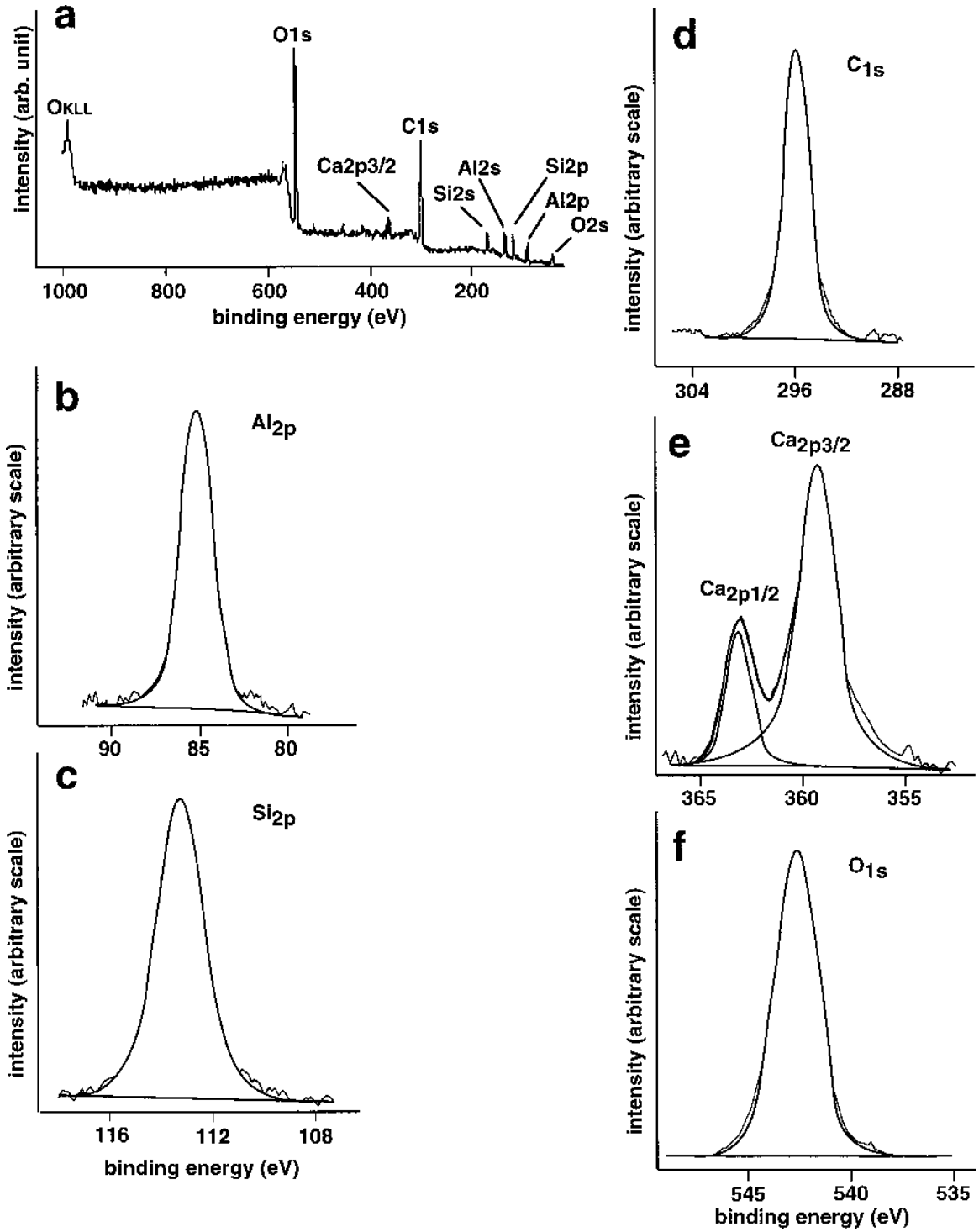

FIGURE 2. Representative spectra of (001) margarite were collected at θ = 45°. (**a**) All the main peaks, including the Auger O KLL peak. The multiple peaks [(**b**) Al2p; (**c**) Si2p; (**d**) C1s; (**e**) Ca2p; (**f**) O1s] are shown after Shirley background subtraction and peak fitting procedure, as light lines. Data are heavy lines.

from the 1s level of C atom in the overlayer, ρ_c is the lateral density of the C in the overlayer, K is the instrumental factor (or spectrometer function) involving the kinetic energy dependence of the spectrometer analyzer transmission function, and $d\sigma_{(C1s)}/d\Omega$ is the differential photoelectric cross-section for the C1s. In solving Equations 1 and 2 we used the values $d_c = 10$ Å and $\lambda_c = 24$ Å.

The instrumental factor is calculated by the general expression

$$K(h\nu) = B_0(h\nu)S_0(h\nu,\theta)\Omega_0(h\nu)F_0 \quad (3)$$

where B_0 is the source brightness, S_0 is the effective source area, Ω_0 is the effective acceptance solid angle, and F_0 is the incident X-ray flux.

The differential photoelectric cross-section for a given subshell is calculated by the general expression

$$\frac{d\sigma_{A,k}}{d\Omega}(h\nu) = \frac{\sigma_{A,k}(h\nu)}{4\pi}[1-\frac{1}{2}\beta_{A,k}(h\nu)(\frac{3}{2}\sin^2\Psi - 1)] \quad (4)$$

where $\sigma_{A,k}$ is the theoretical cross section in square centimeters taken from Yeh and Lindau (1985), $\beta_{A,k}$ is the energy dependent asymmetry parameter of the subshell taken from Yeh and Lindau (1985), ψ is the angle between photon propagation direction and electron emission direction (in the Hewlett-Packard 5950A, ψ is 72°).

We compute the photoemission for each layer and the inelastic attenuation due to all the overlayers above each layer for the maximum depth of 100 monolayers (examples are shown in Fig. 1). The case of a laterally homogeneous emitting layer with uniform overlayers of thickness d_n, which is defined as

$$d_n = d_c + \sum_1^{i-1} d_0 \quad (5)$$

where d_i is the thickness of each layer above the emitting layer, we can use the formalism of Fadley (1978). The dependence of the substrate and overlayer intensities on polar angle θ is expressed as:

$$I_i(A,k,\theta) = K\rho_A \frac{d\sigma_{(A,k)}}{d\Omega}\frac{d_i}{\sin\theta}\exp\{-[i-1(-d_i/\lambda_{A,k}\sin\theta\exp(-d_n/\lambda_n\sin\theta))]\} \quad (6)$$

where I_i (A,k,θ) is the number of photoelectrons per second from the i^{th} layer and from the k^{th} level of atom A, ρ_A is the lateral density of the A element in the i^{th} layer, $\lambda_{A,k}$ is the IMFP from the i^{th} layer and from the k^{th} level of atom A, and λ_n is the electrons IMFP in each of the overlayers calculated by the expression

$$\lambda_n = \frac{\sum_1^{i-1}\lambda_{A,k}}{d_n} \quad . \quad (7)$$

Equation 7 includes the density dependence of $\lambda_{A,k}$. The total intensity from the kth level of atom A is calculated from

$$I_{A,K}(\theta) = \sum_{i=1}^{100} I_i(A,k,\theta). \quad (8)$$

The atom fraction x_A of the A^{th} element of margarite is given by

$$x_A = \frac{I_{A,k,\theta}}{\sum_A I_{A,k,\theta}} \quad (9)$$

where $I_{(A,k,\theta)}$ is the signal intensity as calculated from Equations 6 and 8 having ρ_A as unknown. We chose a depth of 100 monolayers in solving Equation 6, with this being of the same order of 3λ. The calculations were performed assuming the crystal termination could be made either by an Al, Si, or Ca monolayer.

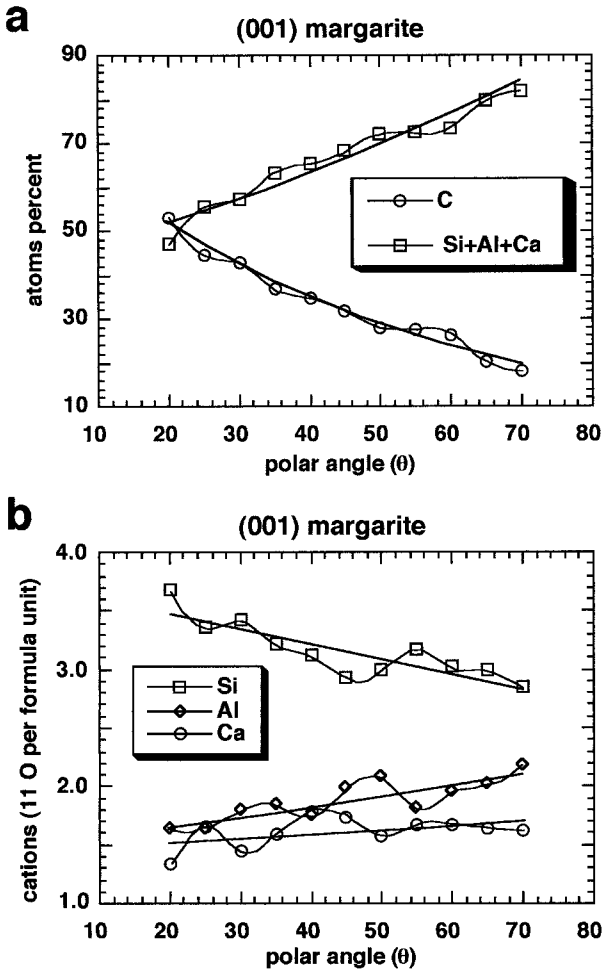

FIGURE 3. Relative concentration vs. polar angle (θ). (**a**) The relationship between C relative concentration and polar angle clearly proves that C is limited to the top most part of the surface. The lack of diffraction modulation suggests that C is amorphous. (**b**) The crystal termination is probably made up of Si. The Ca peak at 25° θ may not be relevant. The cubic spline (light line) and exponential curve (heavy line) fits are also given.

As noted previously, an XPS spectrum is considered as a difference between the background and the measured energy distribution. The background is made up of electrons that underwent multiple elastic and inelastic scattering and should be removed from the peak area pertaining to (the elastic) electrons that escape from the sample without energy losses. Background correction is a very delicate procedure because the tail of each peak is a complex function of elastic and inelastic scattering. Thus elaborate methods to subtract the inelastic background have been proposed (Tougaard 1989; Tougaard and Jansson 1993; Tilinin and Werner 1993). According to Tilinin and Werner (1993), the Tougaard method over- or under-estimates the inelastic background by approximately 5–10%, depending on the emission angle. As a more convenient, but less rigorous, method, we have used the so-called Shirley back-

ground, which should be accurate enough for this ARXPS study. The Shirley background intensity at a given energy is assumed to be proportional to the intensity of the total elastic peak area above the background and to higher kinetic energy. This method implies that each unscattered or elastically scattered electron is associated with a flat background of loss intensity.

Individual peak areas were evaluated by a Voigt peak shape to the elastic intensity and some fitting results of this are shown in Figure 2. These experiment data may have been simply calculated according to

$$x_A = \frac{I_{A,k,\theta} / \alpha_{A,k,\theta}}{\sum_A I_{A,k,\theta} / \alpha_{A,k,\theta}} \quad (10)$$

where $I_{(A,k,\theta)}$ is the experimentally fitted intensity and $\alpha_{(A,k,\theta)}$ is the sensitivity factor. The use of such a ratio obviously implies that the instrumental conditions are constant during the analysis, as was the case in our experiments. The absolute values of $\alpha_{(A,k,\theta)}$ are unimportant, provided that they are all measured under the same conditions. Solving equation 9 (which is more accurate than solving equation 10) and normalizing the cation values to 11 O atoms pfu (i.e., Al + Si + Ca = 7), produced the atomic fractions of Table 2. Following this approach we assume the concentration of oxygen (and discard the analytical data that probably also include contamination due to air-sample interaction). The calculate concentration from the measured intensities should have an accuracy of 2% or better.

RESULTS

The surface chemical composition

XPS provides experimental evidences that surface composition differs from bulk and it is not stoichiometric. The chemical composition does not spread in a way that the electron probe microanalysis bulk composition is the middle point. At high polar angles, the chemical composition trend tends toward stoichiometry, but even the analysis performed at $\theta = 70°$ is still influenced by the anisotropy of the lattice. The dependence of surface composition to polar angle is due to the fact that the depth of analysis decreases with decreasing θ, and elements located in deeper layers are underestimated or no more analyzed. The previous XPS investigation on (001) micas (Biino and Gröning 1998a) also yielded chemical composition far from bulk composition due to presence of interlayered exotic phases, but these margarite crystals do not have interlayered phyllosilicates because no other elements (i.e., Ba, K, Na) were detected. We conclude that due to surface sensitivity of XPS only the topmost layers can be analyzed, and consequently this tool provides useful information on the chemical termination of margarite.

Depth profiling by angle-resolved spectroscopy

Depth profiling by sputtering or etching (intrusive preparation methods) alters the chemistry of the surface. In angle resolved photoelectron spectroscopy, the signal from electrons of a specific energy are collected at varying polar angles and the surface is not perturbed. The angular dependence of intensity provides quantitative information on the chemical gradient perpendicular to the surface because Fadley and Bergström (1971) experimentally proved that enhancement of surface sensitivity by at least one order of magnitude can be achieved by tilting of the sample. Small polar angles ($\theta < 30°$) favor the detection of the topmost surface layers while at large polar angle the topmost surface composition is obscured by the increasing importance of the bulk.

We calculate the escape paths for photoelectrons from the bulk (probing depth) from Equation 6, which includes the relationship between intensity, polar angle, and sampling depth of the photoelectron.

The layered structure of micas is ideal to test the probing depth of ARXPS analysis. Measurements were performed at each 5° polar angle from 20° to 70° (Fig. 3). The topmost layer is clearly made up of C (Fig. 3a). Regardless of whether the crystal termination was assumed to be an Al, Si, or Ca monolayer, the Si concentration increased at low polar angle. Therefore, we performed the full calculation only considering the case of Si terminated structure. Generally, we see that Si increases as take off angle decreases, whereas Al and Ca show opposite effects and very similar behavior. The large variation in intensity cannot be due to the small differences in kinetic energy of Ca, Al, and Si photoelectrons. Therefore, the fact that Si shows a negative slope in Figure 3b implies that Si atoms are preferentially located at or close to surface. Calcium and Al concentrations are decreasing with polar angle, this relationship suggests that they are deeper monolayers. Half of the Al atoms are in the Si monolayer ($^{[4]}$Al) and half in the Al monolayer ($^{[6]}$Al), therefore $^{[4]}$Al photoelectron diffraction should be similar to Si. Consequently $^{[6]}$Al monolayers must be deeper than Ca monolayers to counterbalance the photoelectrons generated by $^{[4]}$Al. The most probable sequence of monolayers in a cleaved (001) margarite thus should be (from top to bottom; Fig. 1) Si-$^{[4]}$Al, O, Ca, O, Si-$^{[4]}$Al, O, and $^{[6]}$Al (our experimental data cannot prove whether O is on top of Si-$^{[4]}$Al or not). It is realistic to assume that steps are present in the analyzed surfaces, but XPS intensities are averages of a large surface area (approximately 1 mm^2) therefore the observed sequence

TABLE 2. Surface chemical composition of (001) margarite by ARXPS

θ	20	25	30	35	40	45	50	55	60	65	70
Si	3.797	3.475	3.539	3.337	3.242	3.050	3.113	3.290	3.138	3.111	2.968
Al	1.749	1.758	1.909	1.962	1.856	2.103	2.197	1.925	2.073	2.134	2.300
Ca	1.454	1.767	1.552	1.701	1.902	1.847	1.690	1.785	1.789	1.755	1.733
C	52.830	44.570	42.571	36.716	34.635	31.725	27.785	27.606	26.392	20.052	18.217
SAC	47.170	55.430	57.429	63.284	65.365	68.275	72.215	72.394	73.608	79.948	81.783

Notes: θ is the polar angle, i.e., the angle between the mineral surface and the analyser. The Si, Al, and Ca cations are normalized to 11 O atoms per formula unit. This normalization did not take into account C. SAC is Si+Al+Ca. Carbon is normalized to 100% of cations.

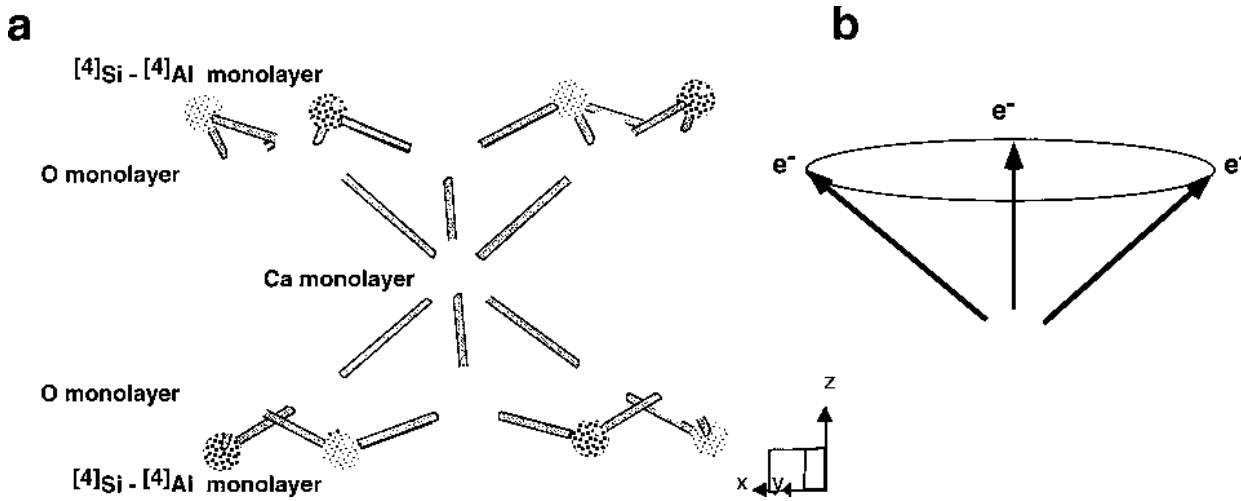

FIGURE 4. (**a**) Part of the margarite structure. [4]Si-[4]Al and O are not on top of Ca. (**b**) The scattering from near-neighbor O is responsible for "channeling" of the outgoing photoelectrons, consequently, modulation in the intensity at ca. 45° polar angle are measured.

of monolayers has only a statistical meaning.

DIFFRACTION EFFECTS

The outgoing photoelectron wave also can be scattered elastically from nearby atoms. Because of the de Broglie wave nature of these electrons, these scattering processes produce an interference or diffraction pattern. The scattering from near-neighbor atoms in the lattice is found to focus the outgoing photoelectron like an optical lens, producing a kind of "forward focusing" or "channeling" of photoelectrons along bond directions or crystallographic axes. At high kinetic energy the scattering is concentrated in the near-forward direction (Fadley 1992). Diffraction effects change the measured peak intensities and they constitute a major source of error in determining surface composition. They are seen in Figure 3b as small modulation in the Si, Al, and Ca intensities of ca. 10–20%. The chemical composition of the surface-near surface region should be calculated after performing measurement over the full solid angle, averaging over azimuthal at each polar angle and than introducing a correction of the diffraction effects by smoothing. Nevertheless, smoothing of a polar scan is enough to provide a reliable chemical composition of the surface-near surface region. A complete data set of measurement (i.e., measurement over the full solid angle) can be exploited to gain the surface structure with an accuracy of 0.05 Å (Fadley 1992; Chamber 1992; Osterwalder et al. 1995). Indeed, some information can already be extracted by a polar scan. Carbon shows very limited scattering effects because the top-most monolayer cannot have forward scattering and C is probably disordered (photoelectron diffraction study of C adatom on phlogopite shows a random distribution of C adatom, Biino et al. submitted). Calcium scattering is negligible at high polar angle, but it becomes very intense at grazing angles. At high polar angle, Ca atoms have no near neighbor atoms that can scatter its photoelectrons. The O atoms in the layer between Si-Al and Ca provide scattering between 15 and 30° (Fig. 4).

The difference between the Al and Si curves permit tracing the different scattering of [6]Al and [4]Al. Taking into consideration the geometrical relationship between the (001) plane, Ca, and the O atoms first neighbor of [6]Al and [4]Al (Fig. 5), we conclude that the oxygen monolayer between [4]Al-[4]Si and Ca is responsible for the low polar angle scattering of the photoelectron generated by [4]Al and [4]Si, and the oxygen monolayers on the top (and on the bottom) of the [6]Al monolayers cause scattering at approximately 45–50° of the photoelectron generated by [6]Al. The apical O of neighbor tetrahedra causes scattering at approximately 50° of the photoelectron generated by [4]Al and [4]Si.

Theoretical polar-angle distribution curves were obtained with the single-scattering calculations model (Cheng et al. 1998). The simulation is based on the bulk lattice model. Comparison between theoretical and experimental polar-angle distribution curves are given in Figure 6. The calculated patterns show a reasonable agreement with experimental data, i.e., the same sequence of ridge and valley but there is no correspondence between theoretical and experimental polar angles. Two main reasons are responsible for the incorrect results. First, the bulk lattice model is probably not accurate due to surface reconstruction and relaxation, second, the correlation between the experimental fine structure emission direction and lattice geometry can be done only after rigorous multiple scattering calculations. The available multiple scattering algorithm (Kaduwela et al. 1991; Cheng et al. 1998) cannot be applied to complex lattices like margarite. Nevertheless, the main theoretical problems are already solved, and in the close future it will be possible to perform multiple scattering calculations of complex minerals.

THE CLEAVAGE MECHANISM

Cleavage of mica should result in the exposure of the interlayer cations according to chemical intuition and rigorous calculations (Giese 1974, 1977, 1978, 1984), but experimental work done on natural muscovite and phengite provides a more complex picture due to interlayered phases (Biino and Gröning

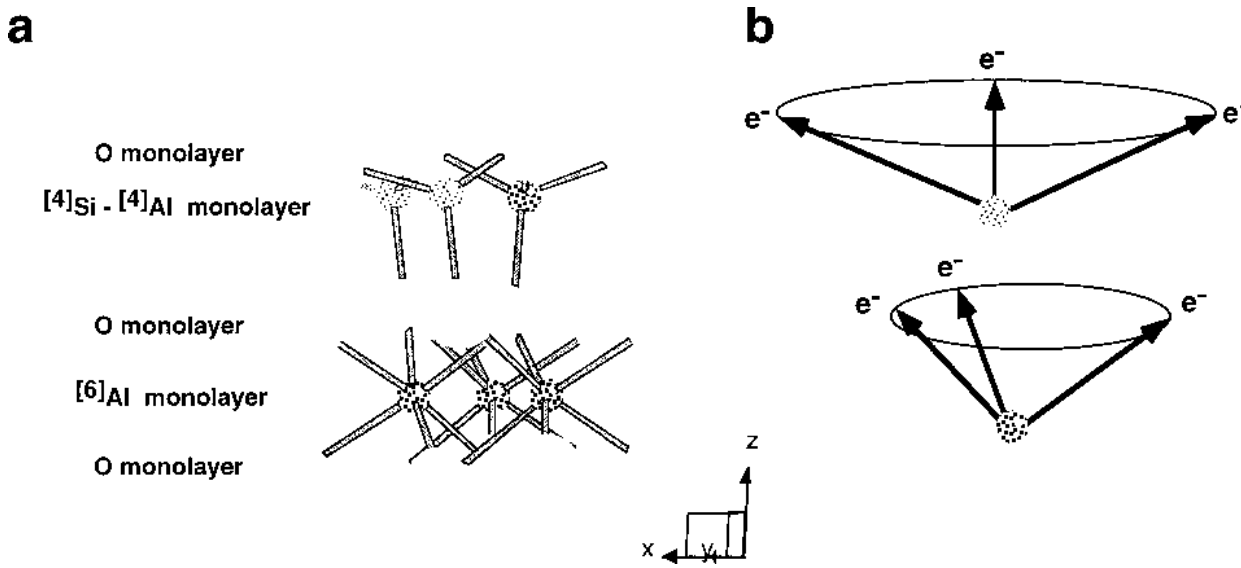

FIGURE 5. (**a**) Part of the margarite structure. Basal O is responsible for low angle diffractions of the photoelectron generated by Si-$^{[4]}$Al atoms. Apical O (not shown) produces scattering close to normal emission ($\theta = 90°$).(**b**) The scattering of the outgoing photoelectrons by the first neighbor O is sketched.

1998a; Biino 1998). A detailed study by Feenstra (1996) suggests that the crystals from this occurrence have no interlayered micas, and we have no evidence for Ba, K, or Na. Chlorite, gibbsite, and kaolinite interlayers will severely change the Ca:Al:Si ratio. Consequently, the Si termination is related to weakness of margarite structure between Si and Al monolayers. The problem of margarite cleavage has never been addressed. From a theoretical point of view, the Ca-O bond is stronger than the K-O bond, and consequently, it is not possible to intuitively conclude that cleavage will expose the interlayer cation without experimental data or theoretical calculation. The net negative charge is physically very close to Ca and the structure may more probably be destabilized between octahedral and tetrahedral sheets.

Our experiments run on margarite provide the evidence for exposure of the Si monolayer (Fig. 3). Two hypotheses can be formulated to explain this observation: the repulsive force between the two negatively charged sheets or imperfections of the natural structure (e.g., vacant cation-exchange sites, stacking faults and/or irregularities in the monolayer stacking). AFM images of micas are generally interpreted as a view of the apical O or of a cation in equivalent position (Lindgreen et al. 1991; Sharp et al. 1993; Eby et al. 1993; Henderson et al. 1994). Indeed, it is improbable according to quantum chemical considerations that O can produce a bump in a AFM image. Our study may suggest that Si is responsible for the bump observed by means of AFM in mica surface images.

DISCUSSION

The (001) surface exposed on cleavage of a margarite single crystal was chemically characterized, for the first time using angle-resolved X-ray photoelectron spectroscopy (ARXPS). The average depth of photoelectron emission is smaller than approximately 30 Å. The probing depth of ARXPS is related to the distance that photoelectrons can travel in the solid, varying the polar angle reduces the lengths of the escape paths for photoelectrons. Surface enhancement was achieved by measuring at 20° polar angle that corresponds to approximately 10 Å of sampling depth. At each polar angle, the surface composition differs from the bulk stoichiometry because the surface composition in a layered structure depends on the arrangement of elements in the layers. The layered structure of micas and the surface sensitivity of ARXPS prevent the sampling of the volume representative of the bulk, as already proposed by Biino and Gröning (1998a). Consequently, ARXPS provides a valuable tool to investigate cleavage of micas. After cleavage, as the Si concentration is constantly rising when the polar angle is decreasing, this monolayer should make the crystal termination. This result is in agreement with a consideration of electrostatic interactions, i.e., repulsion between tetrahedral and octahedral sheet.

Elastic scattering (photoelectron diffraction) effects are not very pronounced, but they change the peak intensities and smoothing of the data is necessary. The approach used to convert the measured intensities into concentration is thus simplistic because it does not take into account the azimuthal angle dependence of the recorded signal, and that the escape probability is function both of elastic and inelastic scattering of electrons. In a more general way, the intensity of the photoelectrons also changes as a function of emission angle due to changes in scattering path length (photoelectron diffraction). However, these effects appear to be no more than 10–20% in magnitude at most. Nevertheless, θ-averaged composition (i.e., after smoothing the diffraction effects) is expected to be accurate in the range of a few percent. The SSC approach has been found to predict some of the features observed experimentally. Indeed, such an approach is not fully adequate, and it is thus necessary to have a multiple scattering algorithm (Kaduwela

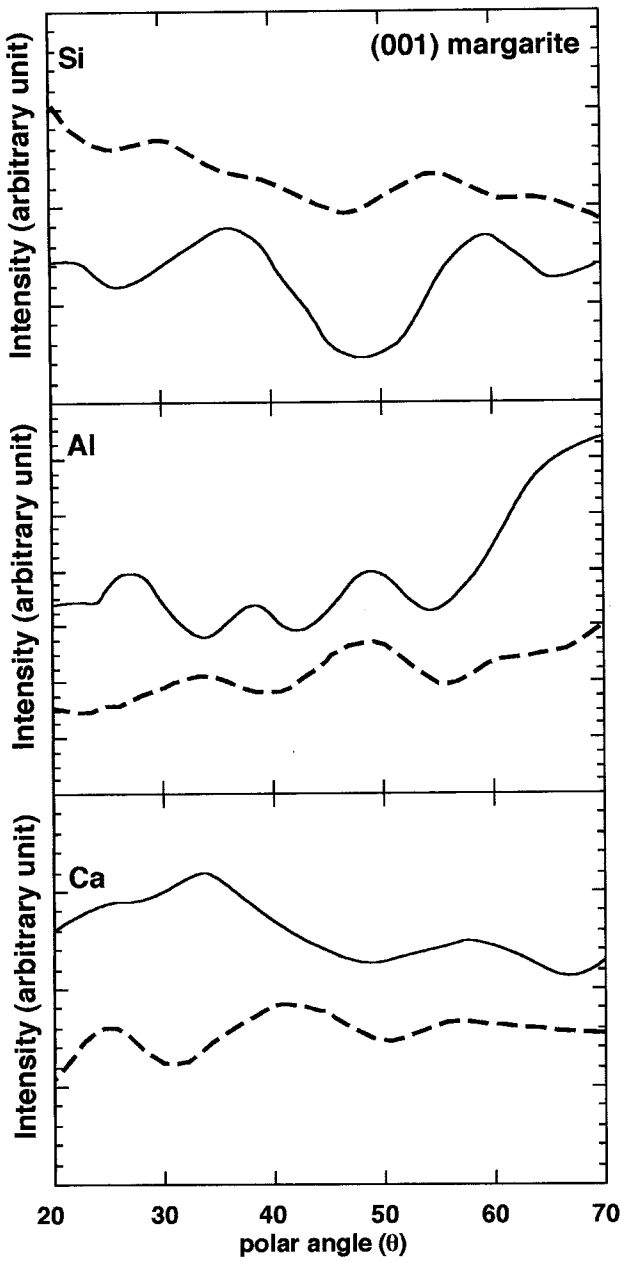

FIGURE 6. Comparison between theoretical (continuous line) and experimental (dashed line) polar-angle distribution curves for various cations.

et al. 1991; Cheng and van Hove in preparation) that can be applied to complex lattices like margarite.

To describe the mechanism of surface reactions on an atomic scale it is necessary to have proper picture of the natural surface. Quantum chemistry simulations of mineral surface are quite popular today, but they are not very efficient if the beginning model is far from reality. The margarite termination is made by Si and from this starting point it is possible to consider sorption-desorption and surface dynamics.

ACKNOWLEDGMENTS

We are indebted to Yufeng Cheng for providing us with phase shifts and the computer program used for the SSC calculation. G.G.B., during this research, was partially supported by a grant of the Swiss National Scientific Foundation. This work was also supported by the U.S. Department of Energy, Office of Energy Research, Basic Energy Science Division, Materials Science Division. At different stages of this work, discussion with J. Abrecht, T. Armbruster, A. Feenstra, P. Gröning, M. Maggetti, and I. Tilinin improved G.G.B. research. G.G.B. gratefully acknowledges the hospitality of the Lawrence Berkeley National Laboratory and of the University of California-Davis. The three anonymous referees and G. Artioli helped to improve clarity of this final version.

REFERENCES CITED

Baird, R.J. (1977) Angular-dependent X-ray photoelectron spectroscopy of solids, 236 p. Ph.D. thesis, University of Hawaii, Honolulu, Hawaii.

Biino, G.G. (1998) X-ray photoelectron spectroscopy (XPS) evidence for interlayer phases in natural micas: effects on physico-chemical properties and geochronological consequences. Schweizerische Mineralogische und Petrographische Mitteilungen, 78, 23–31.

Biino, G.G. and Groening, P. (1998a) Cleavage mechanism and surface chemical characterization of phengitic Muscovite and Muscovite as constrained by X-Ray Photoelectron Spectroscopy. Physics and Chemistry of Minerals, 25, 168–181.

——— (1998b) X-ray photoelectron spectroscopy (XPS) a structural and chemical surface probe: test on aluminosilicate minerals. European Journal of Mineralogy, 33, 423–437.

Biino, G.G., Mun, B., Mannella, N., Kay, A., and Fadley, C.S. (1998): The atomic structure of the surface of (001) phlogopite as revealed by x-ray photoelectron diffraction. EOS, 79/39, 461, 466.

Briggs, D. and Seah, M.P. (1990) Practical surface analysis, Vol. 1 (2nd edition, 2 volumes), 533 p. Wiley, New York.

Bucher, K. and Frey, M. (1994) Petrogenesys of metamorphic rocks, 318 p. Springer Verlag, Berlin.

Bucher-Nurminen, K., Frank, E., and Frey, M. (1983) A model for the progressive regional metamorphism of margarite-bearing rocks in the central Alps. American Journal of Science, 283, 370–395.

Chambers, S.A. (1992) Elastic scattering and interference of backscattered primary, Auger and X-ray photoelectron at high kinetic energy: principles and applications. Surface Science Reports, 16, 261–331.

Chatterjee, N.D. (1974) Synthesis and upper thermal stabillity limit of 2M-margarite $CaAl_2[Al_2Si_2O_{10}/(OH)_2]$. Schweizerische Mineralogische und Petrographische Mitteilungen, 54, 753–767.

——— (1976) Margarite stability and compatibility relations in the system CaO-Al_2O_3-SiO_2-H_2O as a pressure-temperature indicator. American Mineralogist, 61, 699–709.

Chen, Y., Garcia de Abajo, F.J., Chasse, A., Ynzunza, R.X., Biino, G., Rigolini, J., Arenholz, E., Kay, A., Mun, S., Shirley, D.A., Hussain, Z., Van Hove, M.A., and Fadley, C.S. (1998) Cluster-based Methods of Modeling Photoelectron Diffraction Data Using Rehr-Albers Seperable Representation. Violet Ultra-Violet XII International Conference.

Eby, R.K., Henderson, G.S., Wicks, F.J., and Arnold, G.W. (1993) AFM imaging of the crystalline-to-amorphous transition on the surface of ion-implanted mica. Material Research Society Symposium Proceeding, 295, 139–144.

Fadley, C.S. (1978) Basic concepts of X-ray photoelectron spectroscopy. In C.R. Brumble and A.D. Baker, Eds., Electron spectroscopy: theory, techniques and applications, 2, p. 1–156. Academic Press, London.

——— (1992) The study of surface structures by photoelectron diffraction and Auger electron diffraction. In R.Z. Bachrach, Ed., Synchrotron radiation research: advances in surface and interfaces sciences, p. 421–518. Plenum Press, New York.

Fadley, C.S. and Bergström, S.Å.L. (1971) Angular distribution of photoelectrons from a metal single crystal. Physics Letters, 35A, 375–376.

Fadley, C.S., Baird, R.J., Siekhaus, W., Novakov, T., and Bergström, S.Å.L. (1974) Surface analysis and angular distribution in x-ray photoelectron spectroscopy. Journal of Electron Spectroscopy and Related Phenomena, 4, 93–137.

Feenstra, A. (1996) An EMP and TEM-AEM study of margarite, muscovite and paragonite in polymetamorphic metabauxites of Naxos (Cyclades, Greece) and the implications of fine-scale mica interlayering and multiple mica generations. Journal of Petrology, 37, 201–233.

Giese, R.F. (1974) Surfarce energy calculations for muscovite. Nature, 248, 580–581.

———(1977) The influence of hydroxyl orientation, stacking, and ionic substitutions on the interlayer bonding of micas. Clay and Clay Minerals, 25, 102–104.

———(1978) The electrostatic interlayer forces of layer structure minerals. Clay and Clay Minerals, 26, 51–57.

———(1984) Electrostatic energy models of micas. In Mineralogical Society of America Reviews in Mineralogy, 13, 105–144.

Guggenheim, S. (1984) The brittle micas. In Mineralogical Society of America Reviews in Mineralogy, 13, 61–104.

Guggenheim, S. and Bailey, S.W. (1978) Refinement of the margarite structure in subgroup symmetry: correction, further refinement, and comments. American Mineralogist, 63, 186–187.
Henderson, G.S., Vrdoljak, G.A., Eby, R.K., Wicks, F.J., and Rachlin, A.L. (1994) Atomic force microscopy studies of layer silicate minerals. Colloids and Surfaces, 87, 197–212.
Hochella, M.F. Jr., Lindsay, J.R., Mossotti, V.G., and Eggleston, C.M. (1988) Sputter depth profiling in mineral-surface analysis. American Mineralogist, 73, 1449–1456.
Hufner, S. (1996) Photoelectron spectroscopy: principles and applications, 516 p. Springer-Verlag, Berlin.
Junta Rosso, J.L. and Hochella, M.F. Jr. (1996) The chemistry of hematite {001} surfaces. Geochimica et Cosmochimica Acta, 60, 305–314.
Kaduwela, A.P., Friedman, D.J., and Fadley, C.S. (1991) Application of a novel multiple scattering approach to photoelectron diffraction and Auger electron diffraction. Journal of Electron Spectroscopy and Related Phenomena, 57, 223–278.
Lindgreen, H., Garnæs, J., Hansen, P.L., Besenbacher, F., Lægsgaard, E., Stensgaard, I., Gould, S.A.C., and Hansma, P.K. (1991) Ultrafine particles on North Sea illite/smectite clay minerals investigated by STM and AFM. American Mineralogist, 76, 1218–1222.
Martin, C., Arakawa, E.T., Callcott, T.A., and Ashley, J.C. (1985) Low energy electron attenuation length studies in thin amorphous carbon films. Journal of Electron Spectroscopy and Related Phenomena, 35, 307–317.
Osterwalder, J., Aebi, P., Fasel, R., Naumovic, D., Schwaller, P., Kreutz, F., Schlapbach, L., Abukawa, T., and Kono, S. (1995) Angle-scanned photoelectron diffraction. Surface Science, 333, 1002–1014.
Pauling, L. (1930) The structure of the micas and related minerals. Proceedings of the National Academy of Science, U.S.A., 16, 123–129.
Penn, D.R. (1987) Electron mean-free-path calculations using a model dielectric function. Physical Review, 35, 482–486.
Powell, C.J., Jablonski, A., Tanuma, S., and Penn, D.R. (1994) Effects of elastic and inelastic electron scattering on quantitative surface analyses by AES and XPS. Journal of Electron Spectroscopy and Related Phenomena, 68, 605–616.
Seah, M.P. (1990) Charge referencing techniques for insulator. In D. Briggs and M.P. Seah, Eds., Practical surface analysis, 1, p. 541–554. Wiley, New York.
Seah, M.P. and Dench, W.A. (1979) Quantitative electron spectroscopy of surfaces: a standard data base for electron inelastic mean free paths in solids. Surface Interface Analysis, 1, 2–11.
Sharp, T.G., Oden, P.I., and Buseck, P.R. (1993) Lattice-scale imaging of mica and clay (001) surfaces by atomic force microscopy using net attraction forces. Surface Science Letters, 284, L405–L410.
Stipp, S.L. and Hochella, M.F. (1991) Structure and bonding environments at the calcite surface as observed with X-ray photoelectron spectroscopy (XPS) and low energy electron diffraction (LEED). Geochimica et Cosmochimica Acta, 55, 1723–1736.
Tanuma, S., Powell, C.J., and Penn, D.R. (1993) Calculations of electron inelastic mean free paths IV. Surface Interface Analysis, 20, 77–89.
Tilinin, I.S. and Werner, W.S.M. (1993) Angular and energy distribution of Auger and photoelectrons escaping from non-crystalline solid surfaces. Surface Science, 290, 119–133.
Tilinin, I.S., Jablonski, A., and Werner, W.S.M. (1996) Quantitative surface analysis by Auger and X-ray Photoelectron Spectroscopy. Surface Science, 52, 193-335.
Tougaard, S. (1989) Practical algorithm for background subtraction. Surface Science, 216, 343–360.
Tougaard, S. and Jansson, C. (1993) Comparison of validity and consistency of method for quantitative XPS peak analysis. Surface and Interface Analysis, 20, 1013–1046.
Wagner, C.D., Passoja, D.E., Hillery, H.F., Kinisky, T.G., Six, H.A., Jansen, W.T., and Taylor, J.A. (1982) Auger and photoelectron line energy relationships in aluminum-oxygen and silicon-oxygen compounds. Journal Vacuum Science Technology, 21, 933–944.
Yeh, J.J. and Lindau, I. (1985) Atomic subshell photoionization cross sections and asymmetry parameters: $1 < Z < 103$. Atomic data and nuclear data tables. Academic Press, 32, 1–155.

MANUSCRIPT RECEIVED MAY 11, 1998
MANUSCRIPT ACCEPTED NOVEMBER 2, 1998
PAPER HANDLED BY GILBERTO ARTIOLI